RSC Advances

PAPER

View Article Online
View Journal | View Issue

Cite this: *RSC Adv.*, 2017, **7**, 23486

Experimental and theoretical investigations on the defect and optical properties of S- and Al-doped GaSe crystals

Changbao Huang, Zhenyou Wang, Youbao Ni, Haixin Wu* and Shijing Chen

Received 24th January 2017
Accepted 3rd March 2017

DOI: 10.1039/c7ra01057e

rsc.li/rsc-advances

A combination of experimental and computational methods was performed to investigate the defect and optical properties of S-doped and Al-doped GaSe crystals. Our experimental and calculated results indicate that the doped S and Al atoms can form S_{Se} and Al_{Ga}^{+} substitutional defects in the layered GaSe structure. The non-isovalent Al_{Ga}^{+} defect can strengthen the chemical bonding within the intralayer and induce complex defects within the interlayer in the layered GaSe structure. Al-doping maximally improves the hardness of GaSe, which makes it a promising nonlinear frequency conversion material in the infrared and THz ranges. The isovalent S_{Se} defect determines the $GaSe_{1-x}S_x$ mixed structure. Calculated results indicate that the refractive index of $GaSe_{1-x}S_x$ decreases with the x value, while the band gap increases. The unique properties of $GaSe_{1-x}S_x$ may make it a potential candidate for double heterojunction photoelectric materials.

Introduction

Layered III–VI materials, such as GaSe, GaS, InSe and GaTe, have attracted increasing interest in photoelectronic devices due to their exotic electronic and optical properties.[1–4] GaSe is a typical layered III–VI material. Each layer of GaSe has hexagonal symmetry and is composed of four atomic Se–Ga–Ga–Se sheets with intralayer covalent bond connections, while interlayer bonds are of weak van der Waals type.[5] Triggered by the discovery of the two-dimensional graphene,[6] the GaSe monolayers have been investigated as quasi-two-dimensional (2D) materials. On the basis of first-principles density functional theory (DFT) calculations, the electronic[4,7–9] and magnetic properties[10,11] were studied to explore their promising applications in field-effect transistors, heterostructures and spintronics devices. Experimentally, the GaSe monolayers have been fabricated by using micromechanical[12] and van der Waals (vdW) epitaxy techniques,[3] and graphene–GaSe dual heterojunction[13] and GaS–GaSe field-effect transistors[14] have been successfully fabricated. Moreover, due to their excellent optical performances, such as large nonlinear coefficient (75 pm/V) and birefringence (0.34), wide transparency range (0.62–18 μm) and high damage threshold, GaSe crystals have been used to generate coherent lasers in a wide spectral range from the IR to THz regions by nonlinear frequency conversion (NFC).[15–17]

It is well known that the layered GaSe structure can well incorporate different doped elements. Different elements doping have been performed to modify or manipulate the mechanical, optical, electronic, magnetic and electrical properties of GaSe.[18–24] Among these incorporated elements, S- and Al-doping have great attractions. The S-doping allows for control of the electronic, optical properties and lattice strengthening of GaSe within wide ranges.[20,25,26] Moreover, the GaS–GaSe show possibilities in applications of field-effect transistors, photodetectors and photocatalysts.[7,8,14,27] The Al-doping could maximumly improve the microhardness of GaSe crystal, which makes is as promising NFC materials in the IR and THz range.[18–20,28] However, the lower concentration Al-doping (0.5 at%) resulted in the degradation of its optical quality.

The intrinsic and extrinsic defects, which can modify or spoil the performance of materials, play an important role in host structure. It is thus desirable to study the defect information of the doped GaSe in detail. It was experimentally observed that the non-isovalent doped GaSe usually shown deep-level and defect complexes.[24,29,30] Even the Ga excess condition,[31] isovalent Te-doping[32] and In-doping[33,34] in GaSe structure, could form interstitial defects and create donor–acceptor (D–A) pair level of defect complexes. The present work focuses on the experimental and theoretical studies on the defect properties of S-doped and Al-doped GaSe crystals. Based on the results of defect studies, the crystal performances were characterized and predicted by using experimental and theoretical methods.

Experimental and theoretical method

Experimental characterization

Single crystals of pure, S-doped GaSe and Al-doped GaSe were grown by using Bridgman method. The samples were prepared

Anhui Provincial Key Laboratory of Photonic Devices and Materials, Anhui Institute of Optics and Fine Mechanics, Chinese Academy of Sciences, Hefei 230031, China. E-mail: hxwu@aiofm.ac.cn

by cleaving or cutting an ingot along (0001) face. The surface topography of these samples was observed by using a Hitachi SU-8020 scanning electron microscope (SEM) instrument. Raman spectra were recorded by a Raman-Fourier spectrometer LabRam HR Evolution (HORIBA JOBIN YVON) within: $\Delta\lambda$ = 3200–50 cm^{-1} with spectral resolution 0.05 cm^{-1} and 785 nm laser pump. The photoluminescence (PL) measurements were done at 78 K by immersing the samples in liquid nitrogen. A semiconductor laser operating at a wavelength 532 nm was used as a source of excitation. The intensity of the laser beam was 0.02% × 60 mW μm^{-2}. The chemical states of each element in the samples were examined by X-ray photoelectron spectra (XPS) using a Thermo Scientific Escalab 250Xi instrument equipped with a monochromatic Al Kα X-ray source and a hemispherical analyzer. Appropriate electronic charge compensation was employed to perform the analysis and binding energy was referenced to the C-1s peak.

Theoretical calculations

To further understand the defect properties in GaSe system, we performed the first-principles calculations. For this purpose we used density functional theory (DFT) implemented in Quantum ESPRESSO package.[35] The effective ionic potentials[36] were approximated by projector-augmented wave (PAW) method and the valence electron configurations are Ga(3d4s4p), Se(4s4p), S(3s4p) and Al(3s3p). The exchange–correlation energy of electrons was evaluated in the local density approach (LDA) within the Perdew–Wang scheme.[37] The Brillouin-zone integrations were performed using special *k*-point sampling of the Monkhorst-Pack scheme. In all calculations, a 114 Ry energy cutoff and 5 × 5 × 3 *k*-points were used for the 3 × 3 × 1 virgin and defective supercell, which guaranteed the convergence within 0.0002 Ry for total energy. All the structures were relaxed to minimize the total energy of the systems until the residual forces fell below 0.002 eV A^{-1}.

Results and discussions

Experimental analysis

SEM. Unlike the pure and S-doped GaSe crystals, the Al-doped crystals are hard to cleave. Using sharp blade, the (0001) face can be peeled from as-grown boules. Fig. 1 shows the crystal samples (Fig. 1a) and their surface topography of (0001) faces observed by SEM (Fig. 1b–d). The pure and S-doped samples contain complete and smooth (0001) cleaved faces with the size of about ten micrometer. There is no obviously cleaved face in the micro-topography of Al-doped sample: the observed face is rough and uneven compared to these of pure and S-doped samples, which may be due to the strengthening interlayer force.

Raman spectra. Although the layer GaSe crystal is easy to cleave, the strong covalent bonding within its layers make it hard to be pulverized. In our experience, the intensity of XRD peaks related to its (0001) face are very strong, while other peaks are weak or disappear from experimental observations. Here, the Raman spectra were used to investigate the influences of S- and Al-doping on its phase structure. As shown in Fig. 2, the Al-doped and S-doped GaSe samples with low doping concentrations have identical Raman spectra with the pure sample. For the 2.3 wt% S-doped sample, new peaks or splitting peaks are found. It is noted that the XRD data cannot display this difference.[26] Compared the Raman spectra of GaSe with GaS, the newly presented peaks seem to a superposition of the shifted GaSe crystal peak and the GaS peak,[20] which may be due to the mixture of GaSe and GaS structure.

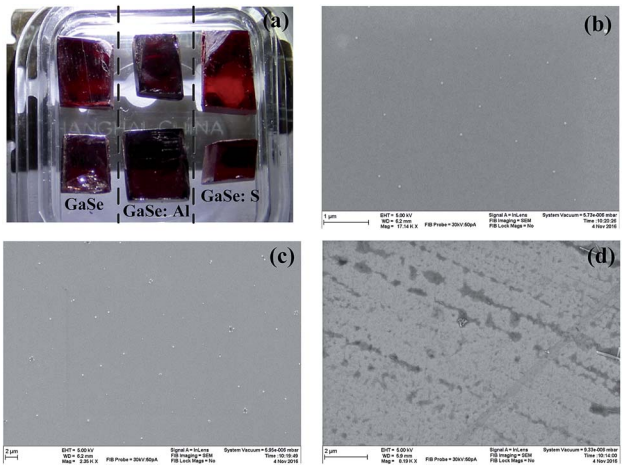

Fig. 1 (a) Photograph of single crystal samples; SEM pictures with ten micrometer size of (b) pure, (c) S-doped (2.3 wt%) and (d) Al-doped (0.23 wt%) GaSe crystal samples.

PL spectra. Fig. 3 shows the PL spectra of pure, Al-doped and S-doped GaSe samples at 78 K. The LA emission band is attributed to the recombination of the direct free exciton. The LB emission band of pure sample has been identified for the recombination of the direct exciton bound to acceptor center.[31] For the S-doped samples, the LA peak is shifted to a high energy, and the LA band widens and overlaps with the LB band. For the Al-doped samples, the LB band has the same shape with that of pure sample, but shows broadening and strengthening tendencies with the increase of Al-doping concentrations. The broad LC peak, observed from Al-doped samples, has been already observed in GaSe crystals with excess Ga,[31] Te-doped[32]

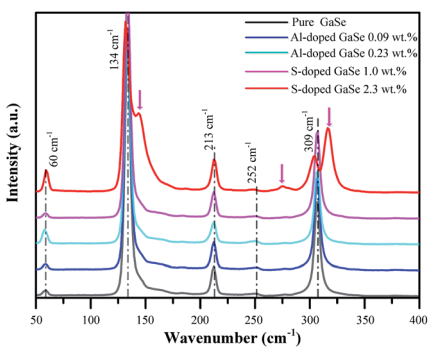

Fig. 2 Raman spectra of pure, S-doped (1.0, 2.3 wt%) and Al-doped (0.09, 0.23 wt%) GaSe crystal samples.

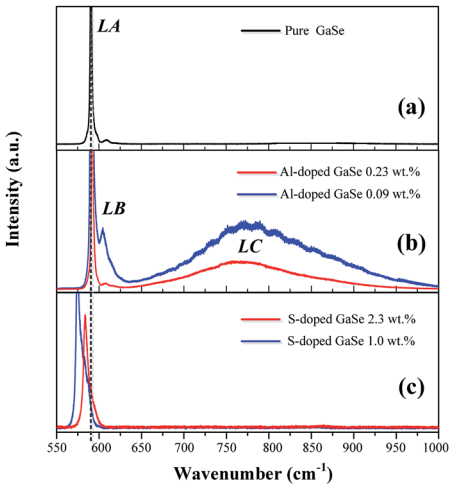

Fig. 3 PL spectra of (a) pure, (b) S-doped (1.0, 2.3 wt%) and (c) Al-doped (0.09, 0.23 wt%) GaSe crystals at 78 K.

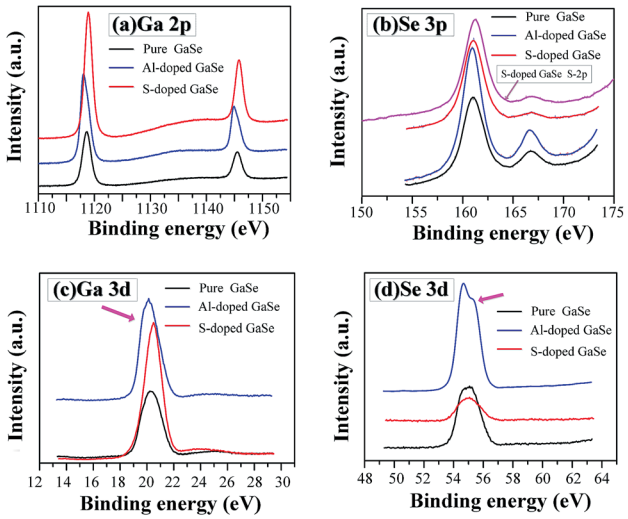

Fig. 4 XPS spectra of (a) Ga-2p, (b) Se-3p, (c) Ga-3d and (d) Se-3d in the pure, S-doped (2.3 wt%) and Al-doped (0.23 wt%) GaSe crystal samples.

and In-doped[33] atoms. Moreover, the broad LC emission band strengthens with the increase of Al-doping concentrations. But the position of LC peak is shifted to low energy compared to other doped samples. The broad LC peak is attributed to the donor–acceptor pair luminescence. It is generally accepted that the major acceptor defects are gallium vacancies V_{Ga} in GaSe crystals.

The Al ion has charge of plus three in stable Al_2Se_3 compound, while Ga ion forms $(Ga–Ga)^{4+}$ dimer unit in the GaSe.[5] Therefore, the Al atoms embed in GaSe layer structure as substitutional defect Al_{Ga}^{1+} or interstitial defect Al_i^{3+}. The positive centers Al_{Ga}^{1+} may induce compensation defects of V_{Ga}^{2-} or Se_i^{2-} and form defect complexes in the GaSe structure. The densities of the defect complexes increase with Al-doping concentrations, which leads to the strengthening of LB and LC band as mentioned above. Both GaS and GaSe have the same layer structure and valence states of elements. Doped with S, the positions of Se atoms are occupied by S atoms, and the S_{Se} defect is non-radiative centers. The shifting and widening of LA band in S-doped sample may be induced by the non-coincidence of covalent radii and electron affinity between S atom and Se atoms. This explains why the S-doping has high concentrations in GaSe structure.

XPS. To further determine the defect types in the doped GaSe structure, the chemical state of Ga and Se in GaSe crystals was investigated by means of XPS (Fig. 4). Fig. 4a shows the Ga-2p XPS spectra of the pure, S-doped (2.3 wt%) and Al-doped (0.23 wt%) GaSe samples. For the pure samples, two peaks are centered at 1145.58 eV and 1118.68 eV, assigned to Ga $2p^{3/2}$ and $2p^{1/2}$ states, are observed in its Ga-2p XPS spectra. Similar peaks were detected for doped samples but with a positive shift of peaks in S-doped sample and a negative shift of peaks in Al-doped sample compared to these of pure sample. The same trend is also observed in Se-3p and Ga-3d states. This signifies that S-doping or Al-doping changes the chemical bond or chemical surrounding in the GaSe structure. The S-doped sample has the similar peaks of Ga-2p, Se-3p, Ga-3d and Se-3d states with the pure sample. Moreover, there is almost overlap between Se-3p and S-2p states in S-doped sample (Fig. 4b). According to ref. 38, the top of valence band and bottom of conduction band of GaSe are formed by a strong mixture of Ga-3s and Se-3p states. Therefore, the S atom substitute Se atom and form $GaSe_{1-x}S_x$ layer structure, which is coincident with the measurements of PL.

It is noted that trace amounts of Al atoms cannot be detected by XPS in the 0.23 wt% Al-doped sample. However, the effects of Al-doping on chemical states in the GaSe structure can be observed from the Se-3d and Ga-3d XPS spectra. Usually, the $3d^{5/2}$ and $3d^{3/2}$ peaks of Ga and Se atoms do not split in GaSe crystal.[39] For the pure and S-doped samples, the 3d peaks (Fig. 4c and d) of Ga and Se atoms preserve the basic symmetry, which are identical to those of unoxidized GaSe reported in ref. 39 and 40. For the Al-doped sample, the Se-3d peak demonstrates the obvious dissymmetry and can be resolved into two overlapping peaks. This may be due to the changes of Se chemical states. On one hand, the substitution of Al^{3+} on one ion of $(Ga–Ga)^{4+}$ dimer units leads to a change of valence state of Se. On the other hand, the interlayer interstitial atoms form chemical bonding with Se atom in the layer structure of GaSe. The mixed valent Se may result in the dissymmetry or separation of Se-3d XPS peak in the Al-doped sample. As with the influence of oxidation states of Ga (Ga_2O_3) on Ga-3d state in GaSe structure,[39] the substitutions of Al_{Ga}^{1+} may induce the change of Ga chemical state, from Ga^{2+} to Ga^{3+}, and result in the slight dissymmetry of Ga-3d XPS peak (Fig. 4c).

Calculated results

Formation energy

We describe the formation energies of different defects to find out which defect is more likely to be present in doped GaSe. The formation energy of a defect D in charge state q is defined as[41]

$$E^{f}(D^{q}) = E_{tot}(GaSe:D^{q}) - E_{tot}(GaSe) - \sum\nolimits_{X} n_X \mu_X + q(E_F + E_{VBM} + \Delta E_{VBM}) \quad (1)$$

$E_{tot}(GaSe:D^q)$ and $E_{tot}(GaSe)$ are the total energies of the supercell with and without the dopant D in the charge state q; E_{VBM} is the valence band maximum (VBM) and E_F is the electron Fermi level with respect to E_{VBM}, while ΔE_{VBM} aligns the E_{VBM} in the supercell with and without the dopant; the integer n_X is the number of atoms of type X (here X = Ga, Se, S, or Al) that are removed from (n_X < 0) and/or added to (n_X > 0) the virgin supercell to form the defect structure, while μ_X is the corresponding chemical potentials of these species. Here, the electron Fermi energy E_F can vary between VBM and conduction band minimum (CBM) of defective systems.

The chemical potential $\mu_X = \mu_X^{elem} + \Delta\mu_X$, is restricted by the following equilibrium conditions: $\Delta\mu_{Ga} + \Delta\mu_{Se} = \Delta G_f(GaSe)$ to maintain a stable compound; $\Delta\mu_{Ga} + \Delta\mu_S \leq \Delta G_f(GaS)$ and $3\Delta\mu_{Al} + 2\Delta\mu_{Se} \leq \Delta G_f(Al_2Se_3)$ to avoid the formation of secondary phases between the host elements and impurities; $\Delta\mu_{Al}$ and $\Delta\mu_S \leq 0$ to prevent precipitation of the elemental solids (S or Al). Here ΔG_f is the calculated Gibbs energy of formation: $\Delta G_f(GaSe) = -1.17$ eV (which is closed to other theoretical value −1.12 eV (ref. 34)), $\Delta G_f(GaS) = -1.36$ eV and $\Delta G_f(Al_2Se_3) = -0.60$ eV. For GaSe under Se-rich (Ga-poor) condition, $\Delta\mu_{Ga}$ and $\Delta\mu_{Se}$ are equal to 0 eV and −1.17 eV respectively; under Ga-rich (Se-poor), $\Delta\mu_{Ga}$ and $\Delta\mu_{Se}$ are equal to −1.17 eV and 0 eV respectively. The thermodynamic transition level $\varepsilon(q_1/q_2)$ is defined as the Fermi-level position for which the formation energies of charge states q_1 and q_2 are equal:

$$\varepsilon(q_1/q_2) = \frac{E^{f}(D^{q_1}; E_F = 0) - E^{f}(D^{q_2}; E_F = 0)}{q_2 - q_1} \quad (2)$$

here $E^f(D^q;E_F = 0)$ is the formation energy of the defect D in the charge state q when the Fermi level is at the VBM. For Fermi-level positions below $\varepsilon(q_1/q_2)$, charge state q_1 is stable, while for Fermi-level positions above $\varepsilon(q_1/q_2)$, charge state q_2 is stable.

Although the LDA can successfully predict the ground-states properties of semiconductors, the shortcoming of LDA leads to the underestimations of energy gaps or Fermi-levels of semiconductors. Presently, the Fermi-level is set between 0 and experimental energy gap (2.12 eV at 77 K (ref. 38)). Schematic diagrams of the defect formation energies as a function of the Fermi-level position and for stable charge-states q are shown in Fig. 5. From the trend of the calculated formation energy in pure, S-doped and Al-doped GaSe, we found the following conclusions:

Intrinsic defects. Under Se-rich condition (Fig. 5a), the formation energy of vacancy Ga (V_{Ga}) is lower than that of Se interstitial (Se_i). It is thermodynamically preferable for V_{Ga} defect rather than Se_i defect under Se-rich growth condition. The Ga vacancy (V_{Ga}) may produce −2 or −3 charge state defect center. Under Ga-rich condition (Fig. 5b), the defects with the lowest formation energies are: interstitial Ga (Ga_i^{2+} or Ga_i^{3+}) for 0 eV ≤ E_F ≤ 0.58 eV, V_{Se}^{2+} for 0.58 eV ≤ E_F ≤ 0.67 eV and V_{Ga}^{2-} for 0.67 eV ≤ E_F ≤ 2.12 eV. The Fermi-level E_F depends on the factors of temperature and chemical environment. The Ga_i^{2+}, V_{Se}^{2+} and V_{Ga}^{2-} may exist in GaSe under Ga-rich condition, which may induce the donor–acceptor pair luminescence. This explains why the Ga excess and Se excess samples have different photoluminescence spectra reported in ref. 31. Therefore, the calculated results indicate that Se-rich condition is good for the growth of GaSe crystal, which is coincident with experiment.[42]

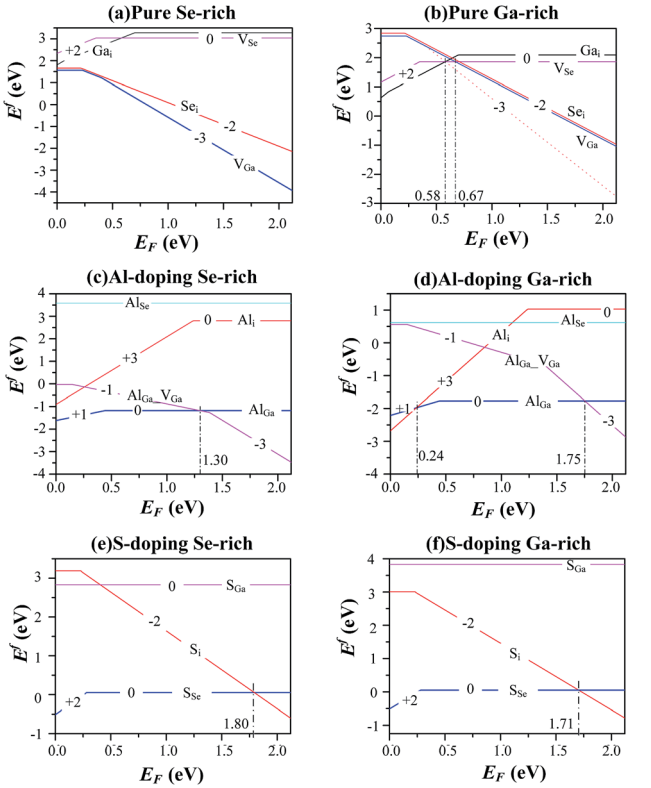

Fig. 5 Schematic diagrams of the formation energies E^f as a function of the Fermi-level E_F position and for stable charge-states q. E^f of (a) and (b) intrinsic defects, (c) and (d) Al impurity, (e) and (f) S impurity under Ga-rich and Se-rich conditions, respectively.

S-induced defects. Under Se-rich condition (Fig. 5e), the defects with the lowest formation energies are: the S_{Se} defect for 0 eV ≤ E_F ≤ 1.80 eV and S_i^{2-} defect for 1.80 eV ≤ E_F ≤ 2.12 eV. Under Ga-rich condition (Fig. 5f), the defects with the lowest formation energies are: the S_{Se} defect for 0 eV ≤ E_F ≤ 1.71 eV and S_i^{2-} defect for 1.71 eV ≤ E_F≤ 2.12 eV. Our calculated E_F and band gap of pure GaSe are 0.35 eV and 0.72 eV respectively. The most stable defect for a wide range of E_F is S_{Se} defect. Considering the influence of temperature and doped defect on E_F, we assume that the S_{Se} is stable defect in S-doped system, which is in accordance with the measured results of PL and XPS. Further discussions would be performed in the calculations of electronic structure and density of state.

Al-induced defects. Under Se-rich condition (Fig. 5c), the formation energy of Al_{Ga} is much less than other defects, indicating that the Al_{Ga} is stable defect. Under Ga-rich condition (Fig. 5d), the defects with the lowest formation energies are: the Al_i defect for 0 eV ≤ E_F ≤ 0.24 eV and Al_{Ga} defect for 0.24 eV ≤ E_F ≤ 2.12 eV. As mentioned above, the non-isovalent substitutions of Al_{Ga}^{1+} may induce compensation defects of V_{Ga}^{2-} or Se_i^{2-} and form defect complexes in the GaSe structure. Therefore, we

calculated the format energies E^f of defect complexes of Al_{Ga}_V_{Ga} and Al_{Ga}_Se_i. Our calculated $E^f(Al_{Ga}\_V_{Ga})$ and E^f $(Al_{Ga}\_Se_i)$ are 2.03 eV and 1.37 eV respectively. The $E^f(Al_{Ga})$, $E^f(V_{Ga})$ and $E^f(Se_i)$ are −0.30 eV, 2.74 eV and 1.66 eV. The complex binding energy $E_b(Al_{Ga}\_V_{Ga}) = E^f(Al_{Ga}) + E^f(V_{Ga}) - E^f(Al_{Ga}\_V_{Ga}) = 0.41$ eV; $E_b(Al_{Ga}\_Se_i) = E^f(Al_{Ga}) + E^f(Se_i) - E^f(Al_{Ga}\_Se_i) = -0.01$ eV. Therefore, the defect complexes of $Al_{Ga}\_V_{Ga}$ are thermodynamically advantageous. Fig. 5c and d displays schematic diagrams of $E^f(Al_{Ga}\_V_{Ga})$ as a function of E_F. The Ga-rich condition produces more types of defects. The stable Al_i^{3+} defect, when E_F < 0.24 eV, could forms new chemical bonds between interlayer in GaSe layer structure.

Electronic properties

Supercell calculations produce folding and complicated electronic band structure (EBS), which makes it difficult to assess the influence of defect perturbations on the EBS of GaSe. In this work, we unfolded the EBS of defective supercell into that of primitive cell (PC) by using BandUp code.[43,44] Fig. 6 shows the EBS for the case of the (a) S_{Se} and (b) $Al_{Ga}\_V_{Ga}$ systems. The color scale represent the number of PC bands crossing, which depends on the Bloch state of wave vector $\boldsymbol{k_i}$ and eigenvalue ε_i.

The orbital character of S_{Se} supercell (Fig. 6a) is similar to these of virgin supercell and GaSe PC which has been described in ref. 38.

In order to understand the nature of S_{Se} defect further, we plot the project density of states (DOS) of S and Se atom in S_{Se} system, as shown in Fig. 7a. Despite the large different in radius and electro-negativity between S and Se atoms, a good match between the orbitals of isovalent S and Se ions produces the similar EBS of S_{Se} system with that of pristine GaSe, which is in accordance with the measured results of XPS. The S-doping does not induce new defect states in the band gap, but increases the band gap value.

Compared to the pristine GaSe EBS, the PC eigenvalues are smeared by the embed defects in $Al_{Ga}\_V_{Ga}$ defective system. Moreover, the $Al_{Ga}\_V_{Ga}$ defects make the Femi-level move downward in the V_{Ga} system. There are three new states appear in the gap: D_1 above and D_2, D_3 below Femi-level. The unoccupied defect state of D_1 may come from the conduction band formed out of Se-p orbitals, while D_2 and D_3 may split off from the rest of the valence bands. Moreover, the defect state induced by interstitial defect Al_i is located in the gap, as shown in Fig. 7b.

Crystal performances

In layer GaSe structure, the cation–cation bonds are along the z crystallographic axes and at about 120-degree angle to cation–anion bonds. As shown in Fig. 8, the S-doping and Al-doping decrease the bonding length in the hexagonal units. The incorporations of S and Al atoms could strengthen the intralayer chemical bonding of layer GaSe structure and improve its micro-hardness. Moreover, the new chemical bonds between interlayer formed by Al_i^{3+} defect can strengthen the interlayer force and further improve the mechanical performance of GaSe crystal. The calculated results demonstrate that the Se-rich condition is good for the growth of Al-doped GaSe crystals. By

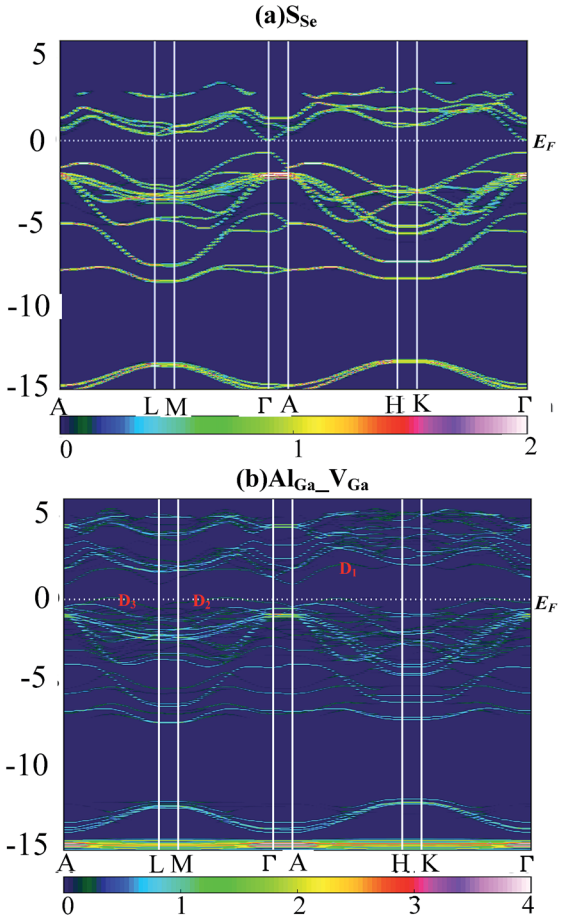

Fig. 6 Electronic band structure of supercell unfolded by using BandUp code: (a) S_{Se} and (b) $Al_{Ga}\_V_{Ga}$ system.

using modified Bridgman method with Se-rich condition, we have successfully grown large size $Ga_{0.49}Se_{0.50}$:0.15 wt% Al (Fig. 9a) and $Ga_{0.49}Se_{0.50}$:0.35 wt% Al (Fig. 9b) single crystals, which possess indentation hardness of 2.27 GPa and 2.79 GPa, respectively, compared to 0.87 GPa of pure GaSe crystal. The $Ga_{0.49}Se_{0.50}$:0.35 wt% Al sample can be cut and polished with any orientation, as shown in Fig. 9b. However, the higher concentration Al-doping may produce the complex defect associations and spoil the optical performance of GaSe (Fig. 9c).

The frequency dependent dielectric permittivity can be described as follow:

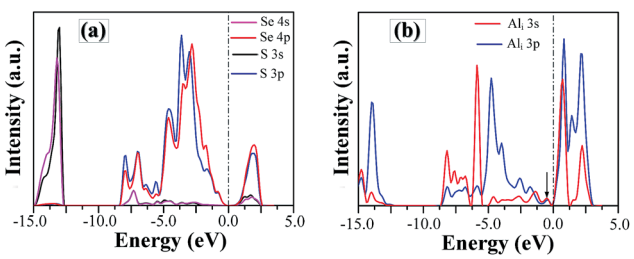

Fig. 7 The project density of states of (a) S and Se atoms in S_{Se} system and (b) Al atom in Al_i system.

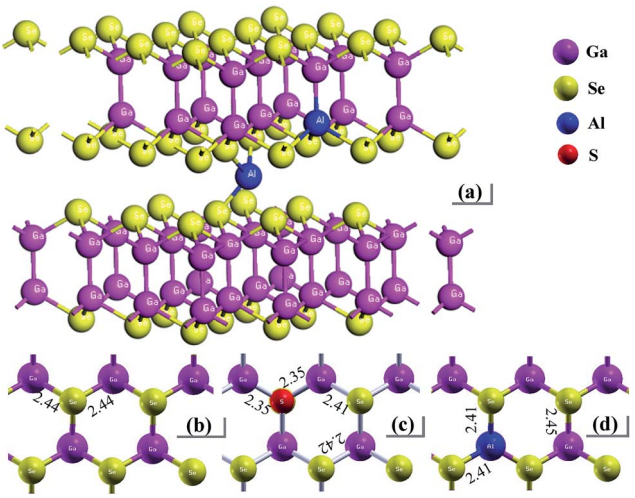

Fig. 8 Schematic view of (a) Al-doped GaSe system including Al^{3+} interstitial defect and Al_{Ga} defect, and plan view and bonding length of a layer in (b) virgin, (c) S_{Se} and (d) Al_{Ga} systems.

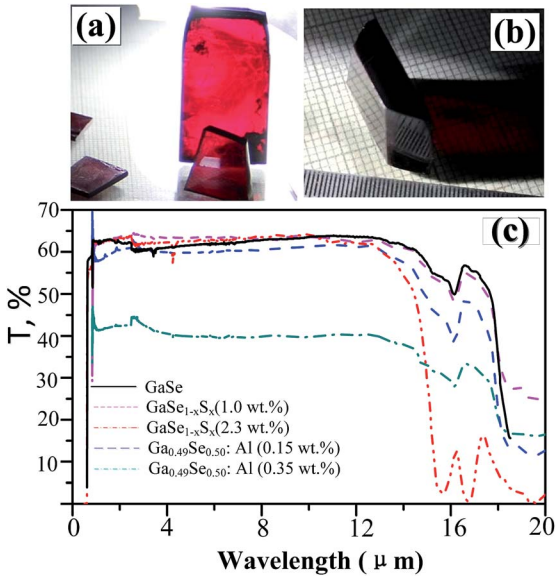

Fig. 9 (a) $Ga_{0.49}Se_{0.50}$:0.15 wt% Al and (b) $Ga_{0.49}Se_{0.50}$:0.35 wt% Al single crystal samples. (c) Full range transparency spectra in infrared range of pure and doped GaSe crystal.

$$\varepsilon_{\alpha\beta}(\omega) = \varepsilon_{\alpha\beta}(\infty) + \frac{4\pi}{\Omega_0}\sum_m \frac{S_{m,\alpha\beta}}{\omega_m{}^2 - \omega^2}. \quad (3)$$

$\varepsilon_{\alpha\beta}(\infty)$ is high-frequency dielectric function which represents the electronic contribution to $\varepsilon_{\alpha\beta}(\omega)$. The second item on the right-hand side represents the phonon oscillator contribution to $\varepsilon_{\alpha\beta}(\omega)$, where $S_{m,\alpha\beta}$ is the mode oscillator strength tensor which is related to ionic displacements and Born effective charge tensors, ω_m is the phonon eigen-frequency. In the transparent range, the refractive index of semiconductor (non-ferromagnetic material) is given as $n = (\varepsilon_{\alpha\beta})^{1/2}$. Fig. 10 displays frequency dependent refractive indexes of GaSe and GaS calculated by using ABINIT code with density functional

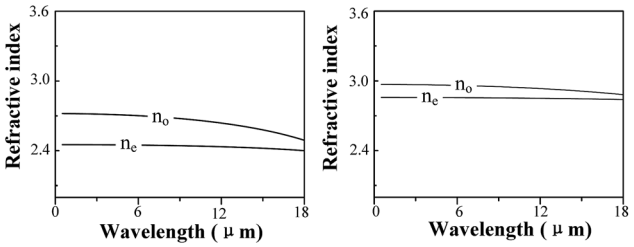

Fig. 10 Refractive indexes of (a) GaS and (b) GaSe calculated by using the DFPT method.

perturbation theory (DFPT).[45] The phonon effects make the dispersion curves slope downward. The refractive index of GaSe is 0.3 bigger than that of GaS. The refractive index of $GaSe_{1-x}S_x$ decreases with x value, while the band gap increases with x value. The unique properties of $GaSe_{1-x}S_x$ may make it potential candidates for double heterojunction photo-electric materials. The $GaSe_{1-x}S_x$ material can provide potential well/barrier, and the GaSe can be performed as the waveguide and active materials. The depth of potential well can be adjusted by changing the x value. The band gap value of GaSe can be manipulated by adjusting the number of layer and mechanical strain.[8,9]

Conclusions

A combination of experimental and computational methods was performed to investigate the defect and optical properties of S-doped and Al-doped GaSe crystals. The measurements of PL, XPS and SEM indicate that S atoms form S_{Se} substitutional defect, and Al atoms could induce complex defects of $Al_{Ga}{}^{+}$ and the interlayer interstitial atoms. Results of defect formation energy calculations are in accordance with experimental measurements for the doped defect types. The calculations of electronic properties (EBS and DOS) reveal the defect levels of Al-doped systems. Moreover, the calculated results indicate that the Se-rich condition is good for the growth of Al-doped GaSe crystals. Based on these calculations, we successfully grown Al-doped GaSe crystals with higher hardness and optical quality. Attracted by the layer $GaSe_{1-x}S_x$ mixture structure, we investigate its dielectric properties by using DFPT, which reveals that the refractive index of $GaSe_{1-x}S_x$ decreases with x value.

The significantly improved hardness of Al-doped GaSe crystal make it more propitious to be cut and polished with specific orientation for use, which could improve the laser conversion efficiency. Therefore, the Al-doped GaSe crystal can be used as promising nonlinear frequency conversion materials in the infrared and THz ranges. The energy gap and refractive index of $GaSe_{1-x}S_x$ can be controlled by adjusting S-doping concentrations. The unique properties of $GaSe_{1-x}S_x$ may make it a potential candidate for the double heterojunction photoelectric material.

Acknowledgements

The authors acknowledge financial support from Knowledge Innovation Program of the Chinese Academy of Sciences (CXJJ-

16M128). Part of the calculations was performed in Center for Computational Science of CASHIPS. The atomic structures are visualized using the XCrysDen code.[46] We used the pseudopotentials from the Quantum ESPRESSO pseudopotential data base: http://www.quantum-espresso.org/pseudopotentials.

References

1 K. R. Allakhverdiev, M. Ö. Yetis, S. Ozbek, T. K. Baykara and E. Y. Salaev, *Laser Phys.*, 2009, **19**, 1092–1104.
2 Y. Tang, K. C. Mandal, J. A. McGuire and C. W. Lai, *Phys. Rev. B*, 2016, **94**, 125302.
3 H. Cai, E. Soignard, C. Ataca, B. Chen, C. Ko, T. Aoki, A. Pant, X. Meng, S. Yang, J. Grossman, F. D. Ogletree and S. Tongay, *Adv. Mater.*, 2016, **28**, 7375–7382.
4 D. V. Rybkovskiy, A. V. Osadchy and E. D. Obraztsova, *Phys. Rev. B: Condens. Matter Mater. Phys.*, 2014, **90**, 235302.
5 N. C. Fernelius, *Prog. Cryst. Growth Charact. Mater.*, 1994, **28**, 275–353.
6 K. S. Novoselov, A. K. Geim, S. V. Morozov, D. Jiang, Y. Zhang, S. V. Dubonos, I. V. Grigorieva and A. A. Firsov, *Science*, 2004, **306**, 666–669.
7 W. Wei, Y. Dai, C. Niu, X. Li, Y. Ma and B. Huang, *J. Mater. Chem. C*, 2015, **3**, 11548–11554.
8 Y. Ma, Y. Dai, M. Guo, L. Yu and B. Huang, *Phys. Chem. Chem. Phys.*, 2013, **15**, 7098–7105.
9 D. V. Rybkovskiy, N. R. Arutyunyan, A. S. Orekhov, I. A. Gromchenko, I. V. Vorobiev, A. V. Osadchy, E. Y. Salaev, T. K. Baykara, K. R. Allakhverdiev and E. D. Obraztsova, *Phys. Rev. B: Condens. Matter Mater. Phys.*, 2011, **84**, 085314.
10 L. Ao, H. Y. Xiao, X. Xiang, S. Li, K. Z. Liu, H. Huang and X. T. Zu, *Phys. Chem. Chem. Phys.*, 2015, **17**, 10737–10748.
11 T. Cao, Z. Li and S. G. Louie, *Phys. Rev. Lett.*, 2015, **114**, 236602.
12 L. Quan, Y. Song, Y. Lin, G. Zhang, Y. Dai, Y. Wu, K. Jin, H. Ding, N. Pan, Y. Luo and X. Wang, *J. Mater. Chem. C*, 2015, **3**, 11129–11134.
13 W. Kim, C. Li, F. A. Chaves, D. Jimenez, R. D. Rodriguez, J. Susoma, M. A. Fenner, H. Lipsanen and J. Riikonen, *Adv. Mater.*, 2016, **28**, 1845–1852.
14 D. J. Late, B. Liu, J. Luo, A. Yan, H. S. S. R. Matte, M. Grayson, C. N. R. Rao and V. P. Dravid, *Adv. Mater.*, 2012, **24**, 3549–3554.
15 W. Shi, Y. J. Ding, X. Mu and N. Fernelius, *Appl. Phys. Lett.*, 2002, **80**, 3889.
16 Z. Rao, X. Wang and Y. Lu, *Opt. Commun.*, 2011, **284**, 5472–5474.
17 K. Finsterbusch, A. Bayer and H. Zacharias, *Appl. Phys. B*, 2004, **79**, 457–462.
18 Y.-F. Zhang, R. Wang, Z.-H. Kang, L.-L. Qu, Y. Jiang, J.-Y. Gao, Y. M. Andreev, G. V. Lanskii, K. A. Kokh, A. N. Morozov, A. V. Shaiduko and V. V. Zuev, *Opt. Commun.*, 2011, **284**, 1677–1681.
19 J. Guo, J. J. Xie, L. M. Zhang, D. J. Li, G. L. Yang, Y. M. Andreev, K. A. Kokh, G. V. Lanskii, A. V. Shabalina, A. V. Shaiduko and V. A. Svetlichnyi, *CrystEngComm*, 2013, **15**, 6323.
20 J. Guo, J.-J. Xie, D.-J. Li, G.-L. Yang, F. Chen, C.-R. Wang, L.-M. Zhang, Y. M. Andreev, K. A. Kokh, G. V. Lanskii and V. A. Svetlichnyi, *Light: Sci. Appl.*, 2015, **4**, e362.
21 Z. S. Feng, J. Guo, J. J. Xie, L. M. Zhang, J. Y. Gao, Y. M. Andreev, T. I. Izaak, K. A. Kokh, G. V. Lanskii, A. V. Shaiduko, A. V. Shabalina and V. A. Svetlichnyi, *Opt. Commun.*, 2014, **318**, 205–211.
22 Z. S. Feng, Z. H. Kang, F. G. Wu, J. Y. Gao, Y. Jiang, H. Z. Zhang, Y. M. Andreev, G. V. Lanskii, V. V. Atuchin and T. A. Gavrilova, *Opt. Express*, 2008, **16**, 9978–9985.
23 M. Yüksek, A. Elmali, M. Karabulut and G. M. Mamedov, *Opt. Mater.*, 2009, **31**, 1663–1666.
24 Y.-K. Hsu, C.-S. Chang and W.-C. Huang, *J. Appl. Phys.*, 2004, **96**, 1563.
25 K. A. Kokh, J. F. Molloy, M. Naftaly, Y. Andreev, V. A. Svetlichnyi, G. V. Lanskii, I. N. Lapin, T. I. Izaak and A. E. Kokh, *Mater. Chem. Phys.*, 2015, **154**, 152–157.
26 Y. M. Andreev, V. V. Atuchin, G. V. Lanskii, A. N. Morozov, L. D. Pokrovsky, S. Y. Sarkisov and O. V. Voevodina, *Mater. Sci. Eng. B*, 2006, **128**, 205–210.
27 C. S. Jung, K. Park, F. Shojaei, J. Y. Oh, H. S. Im, J. A. Lee, D. M. Jang, J. Park, N. Myoung, C.-L. Lee, J. W. Lee, J. K. Song and H. S. Kang, *Chem. Mater.*, 2016, **28**, 5811–5820.
28 S. Das, C. Ghosh, O. G. Voevodina, Y. M. Andreev and S. Y. Sarkisov, *Appl. Phys. B*, 2005, **82**, 43–46.
29 S. Shigetomi, T. Ikari and H. Nakashima, *J. Appl. Phys.*, 1993, **74**, 4125–4129.
30 S. Shigetomi, T. Ikari and H. Nakashima, *J. Appl. Phys.*, 1996, **80**, 4779–4781.
31 S. Shigetomi and T. Ikari, *J. Appl. Phys.*, 2003, **94**, 5399–5401.
32 I. Evtodiev, L. Leontie, M. Caraman, M. Stamate and E. Arama, *J. Appl. Phys.*, 2009, **105**, 023524.
33 Y. Cui, R. Dupere, A. Burger, D. Johnstone, K. C. Mandal and S. A. Payne, *J. Appl. Phys.*, 2008, **103**, 013710.
34 Z. Rak, S. D. Mahanti, K. C. Mandal and N. C. Fernelius, *Phys. Rev. B: Condens. Matter Mater. Phys.*, 2010, **82**, 155203.
35 P. Giannozzi, S. Baroni, N. Bonini, M. Calandra, R. Car, C. Cavazzoni, D. Ceresoli, G. L. Chiarotti, M. Cococcioni, I. Dabo, A. Dal Corso, S. de Gironcoli, S. Fabris, G. Fratesi, R. Gebauer, U. Gerstmann, C. Gougoussis, A. Kokalj, M. Lazzeri, L. Martin-Samos, N. Marzari, F. Mauri, R. Mazzarello, S. Paolini, A. Pasquarello, L. Paulatto, C. Sbraccia, S. Scandolo, G. Sclauzero, A. P. Seitsonen, A. Smogunov, P. Umari and R. M. Wentzcovitch, *J. Phys.: Condens. Matter*, 2009, **21**, 395502.
36 N. Troullier and J. L. Martins, *Phys. Rev. B: Condens. Matter Mater. Phys.*, 1991, **43**, 1993–2006.
37 J. P. Perdew and Y. Wang, *Phys. Rev. B: Condens. Matter Mater. Phys.*, 1992, **45**, 13244–13249.
38 Z. Rak, S. D. Mahanti, K. C. Mandal and N. C. Fernelius, *J. Phys. Chem. Solids*, 2009, **70**, 344–355.
39 S. M. Tan, C. K. Chua, D. Sedmidubsky, Z. Sofer and M. Pumera, *Phys. Chem. Chem. Phys.*, 2016, **18**, 1699–1711.
40 F. Marquez, A. Segura, V. Munoz and G. Gonzalez, *Surf. Interface Anal.*, 2002, **34**, 460–463.

41 C. Freysoldt, B. Grabowski, T. Hickel, J. Neugebauer, G. Kresse, A. Janotti and C. G. Van de Walle, *Rev. Mod. Phys.*, 2014, **86**, 253–305.
42 T. Onai, Y. Nagai, H. Dezaki and Y. Oyama, *J. Cryst. Growth*, 2013, **380**, 18–22.
43 P. V. C. Medeiros, S. S. Tsirkin, S. Stafström and J. Björk, *Phys. Rev. B: Condens. Matter Mater. Phys.*, 2015, **91**, 041116.
44 P. V. C. Medeiros, S. Stafström and J. Björk, *Phys. Rev. B: Condens. Matter Mater. Phys.*, 2014, **89**, 041407.
45 M. Veithen, X. Gonze and P. Ghosez, *Phys. Rev. B: Condens. Matter Mater. Phys.*, 2005, **71**, 125107.
46 A. Kokalj, *J. Mol. Graphics Modell.*, 1999, **17**, 176–179.